Bulk-Type Solid-State LIB

Nobuya Machida

Abstract The all-solid-state batteries have the potential advantages of safety performance for an accident such as thermal shock during utilization. In this chapter, we introduce some studies using the bulk-type solid-state test cells as examples for the investigation of electrode materials and electrode composites. $LiAlO_2$ coating on $LiNi_{1/3}Mn_{1/3}Co_{1/3}O_2$ (NMC) was investigated in order to improve the electrochemical properties of the all-solid-state battery using a sulfide-based solid electrolyte amorphous Li_3PS_4. The $LiAlO_2$ coating on NMC powders was carried out by the use of a sol–gel method. A bulk-type solid-state test cell was constructed with the obtained $LiAlO_2$-coated NMC. The charge–discharge cycling test of the cell revealed that the test cell with $LiAlO_2$-coated NMC showed the capacity larger than 124 $mAhg^{-1}$ even after 400 cycles. Incidentally, the amount of solid electrolyte in the composite electrode limits the total energy density of the battery. In order to reduce the solid electrolyte content in the positive electrode composites, we were conducted on the solid electrolyte coating on the active materials NMC by a wet process. The test cell with the Li_3PS_4-coated NMC showed the capacity of $145mAhg^{-1}$, which was calculated on the base of the NMC weight in the composite electrode. The capacity was larger than that of the non-coated NMC. The all-solid-state battery with the Li_3PS_4-coated NMC had larger specific energy density than that with the non-coated NMC with the same Li_3PS_4 content.

Keywords All-solid-state battery · Lithium-ion battery · $LiAlO_2$ coating · Li_3PS_4 coating

1 Introduction

Toward the goal of realizing sustainable and greener energy scenario, economic and efficient energy storage forms a key challenge. In this context, rechargeable lithium-ion batteries have become a frontrunner device empowering small-scale portable

N. Machida (✉)
Faculty of Science, Konan University, Kobe, Japan
e-mail: machida@konan-u.ac.jp

K. Kanamura (ed.), *Next Generation Batteries*,
https://doi.org/10.1007/978-981-33-6668-8_10

electronic devices to large-scale electric vehicles. The solidification of lithium-ion batteries, in which non-flammable lithium-ion conducting solid electrolytes are used, is very useful for improving the safety and reliability of the lithium-ion batteries [1–4]. The all-solid-state batteries have the potential advantages, no leakage of electrolyte solutions, easy miniaturization such as thin-film batteries, and have safety performance for an accident such as thermal shock during utilization. However, there are no commercially available all-solid-state batteries for practical high-power uses. It indicates that the all-solid-state batteries for high power uses are under the stage of research and development. The all-solid-state test cells for the research and developments are roughly divided into two types, (1) bulk-type solid-state test cell and (2) sheet-type solid-state test cell, according to the purpose and stage of the research and developments.

The advantages of the bulk-type test cells are easy assembling and simple cell constitutions. The bulk-type test cells can be assembled by only successive pressing positive electrode composites, solid electrolytes, and negative electrode composites into a pellet. The bulk-type test cells can be also constituted without additives such as polymer binders, which sometimes cause deterioration in the electrochemical properties of the test cells. The bulk-type solid-state test cells, in consequent, are frequently used in order to investigate the electrochemical properties of newly appeared electrode materials and also newly prepared electrode composites for the all-solid-state batteries. The bulk-type test cells are also used to estimate the appropriate loading amount of active materials for the development of the cells with high energy densities. On the other hand, the sheet-type solid-state test cells are prototype batteries for commercially available batteries. The details on the sheet-type cells are described in Chap. 11. In this chapter, some studies using the bulk-type solid-state test cells are introduced as examples for the investigation of electrode materials and electrode composites.

2 Typical Bulk-Type Solid-State Test Cells and Their Properties

In order to improve the electrochemical properties of the all-solid-state battery using sulfide-based solid electrolytes, many studies have been conducted to form an effective electrode–electrolyte interface, because electrochemical reactions occur through the solid–solid interface between the electrode and solid electrolyte materials, and the interface governs the electrochemical properties of the all-solid-state batteries. Coating of lithium-ion conductive oxides, for example, $Li_4Ti_5O_{12}$ and $LiNbO_3$ on positive electrode active materials such as $LiCoO_2$ and $LiNi_{1/3}Mn_{1/3}Co_{1/3}O_2$, has been reported as an effective modification technique [5–11]. Accordingly, $LiAlO_2$ coating on $LiNi_{1/3}Mn_{1/3}Co_{1/3}O_2$ (NMC) was investigated [11].

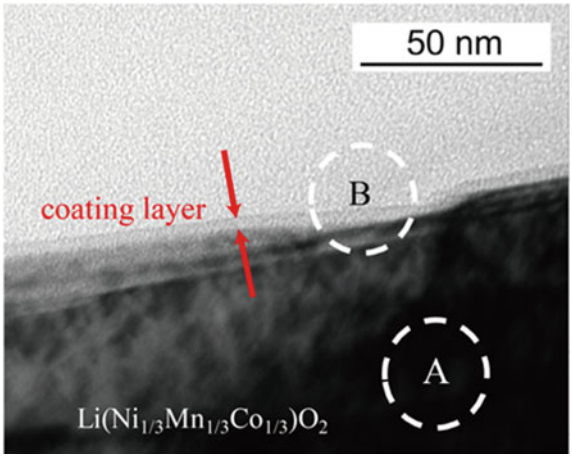

Fig. 1 A TEM image of the 1.0 mol% $LiAlO_2$-coated $LiNi_{1/3}Mn_{1/3}Co_{1/3}O_2$ (NMC) particles annealed at 350 °C. The points for EDX measurements are also shown as dotted circles, A and B, in the figure. Reprinted from Ref. [11], Copyright 2014, with permission from Elsevier

The $LiAlO_2$ coating on NMC powders was prepared by the use of a sol–gel method. The coating sol was prepared from the raw materials, aluminium (III) sec-butoxide, ethyl-acetoacetate, H2O, and 2-propanol. After mixing those raw materials, an appropriate amount of lithium methoxide was added to the mixture, which was stirred continuously at room temperature. NMC powders were added into the coating sol and ultrasonically agitated 40 °C for 30 min. The mixture was concentrated under reduced pressure, and the residual was obtained as a precursor. The $LiAlO_2$-caoted NMC powders were obtained by heat treatment of the precursor at 350 °C. The TEM image of the surface of the 1.0 mol% $LiAlO_2$-coated NMC powder is depicted in Fig. 1. It is clearly seen that the surface of the NMC particle is coated with a homogeneous layer with thickness of 8–15 nm. The TEM observation confirms that the $LiAlO_2$ coating layer is amorphous state. The elemental point analysis using EDX spectroscopy was carried out on the sample. The EDX spectra were measured at positions, A and B, denoted by dotted circles in Fig. 1. The electron beam of about 30 nm in diameter was used for the EDX measurements. The EDX spectrum measured in the surface area B showed a signal of Al element in addition to the signals of Ni, Mn, and Co elements. On the other hand, the signal of Al element cannot be detected in EDX spectrum that has been measured in the bulk area (point A). Those results suggest that the surface of NMC particle has been covered $LiAlO_2$ layer and Al element has not diffused into the inner area of the NMC particles during the heat treatment in the $LiAlO_2$ coating process.

A bulk-type solid-state test cell was constructed with the obtained $LiAlO_2$-coated NMC. A schematic diagram of the bulk-type test cell is shown in Fig. 2. In this case, amorphous Li_3PS_4 was used as a separator of solid electrolytes and $Li_{4.4}Si$ alloy as negative electrode material. The positive electrode of the cell was a mixture of the active material, the $LiAlO_2$-coated NMC (59 wt%), amorphous Li_3PS_4 solid electrolyte (39 wt%) and acetylene black (2 wt%). The cell was prepared by successively

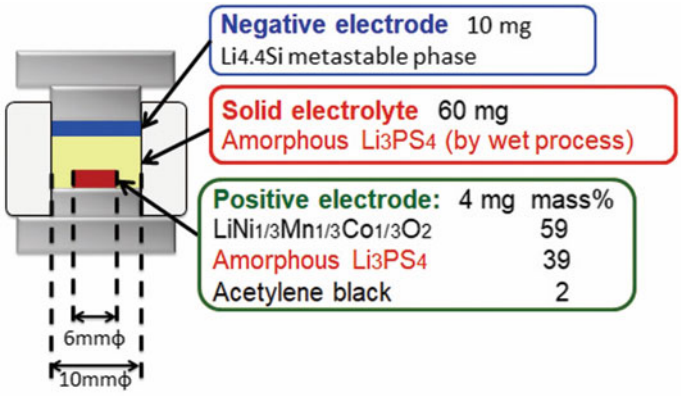

Fig. 2 Bulk-type solid-state cell for electrochemical measurement

pressing the positive electrode mixture, the solid electrolyte powders, and $Li_{4.4}Si$ alloy powders at 380 MPa into a pellet of 10 mm diameter.

The charge–discharge cycling tests of the cells were carried out under a constant current density of 0.1 mA cm^{-2} at 25 °C. In the test, charge–discharge criteria of voltage were set 4.3 and 2.5 V, respectively. Figure 3 shows the charge–discharge curves of the test cell with the 1.0 mol% $LiAlO_2$-coated NMC. The charge–discharge curves of the cell with uncoated NMC are also shown in the figure for comparison. The abscissa of the figure is the capacity calculated on the base of weight of the NMC in the composite electrode. The first discharge capacity of the cell with the uncoated NMC is about 102 $mAhg^{-1}$ and the capacities gradually decreased with an increase in the cycle number. After 100 cycles, the capacity was degraded to

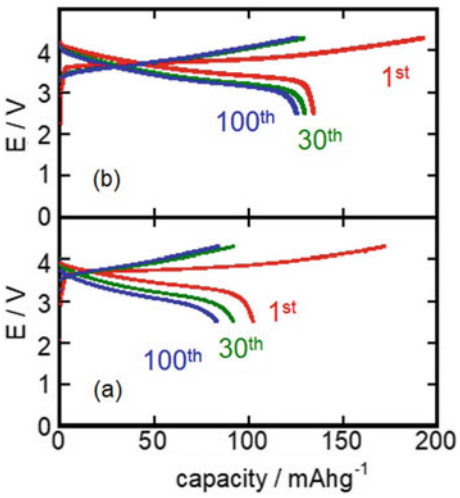

Fig. 3 Charge–discharge curves of the cells $Li_{4.4}Si$ | a-Li_3PS_4 | NMC; **a** the uncoated sample and **b** 1.0 mol% $LiAlO_2$-coated sample. The current density was 0.1 $mAcm^{-2}$. Reprinted from Ref. [11], Copyright 2014, with permission from Elsevier

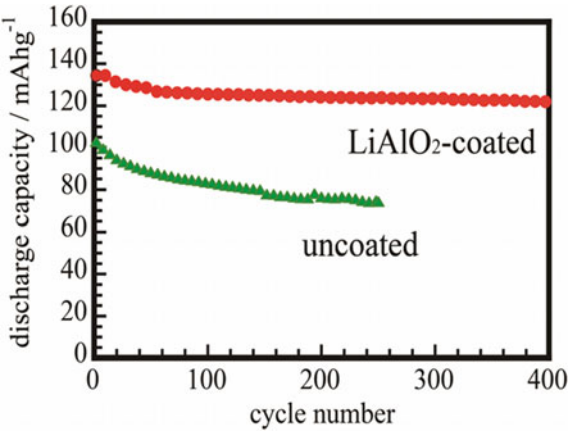

Fig. 4 Cycle performance of the cells $Li_{4.4}Si$ | a-Li_3PS_4 | NMC at the current density of 0.1 $mAcm^{-2}$. The closed triangles denote the cell performance of the uncoated NMC and the closed circles denote the cell performance of the 1.0 mol% $LiAlO_2$-coated NMC. Reprinted from Ref. [11], Copyright 2014, with permission from Elsevier

be 82 $mAhg^{-1}$. On the other hand, the cell with the $LiAlO_2$-coated NMC shows the capacity of 134 $mAhg^{-1}$ for the first cycle. The cell with the $LiAlO_2$-coated NMC keeps the capacity larger than 125 $mAhg^{-1}$ even after 100th charge–discharge cycles. The capacity retention rate after 100 cycles is about 95% for the cell with the $LiAlO_2$-coated NMC.

Figure 4 shows cycle dependence of specific capacities of the bulk-type test cells with the uncoated and the 1.0 mol% $LiAlO_2$-coated NMC as positive electrodes. The first discharge capacity of the cell with the $LiAlO_2$-coated NMC is 134 $mAhg^{-1}$. The discharge capacity is gradually decreasing with an increase in cycle number in the range of 1–50 cycles. After 50 cycles, however, the cell keeps a specific capacity larger than 124 $mAhg^{-1}$ even after 400 cycles. The capacity after 400 cycles is more than 92% of the initial discharge capacity. On the other hand, the cell with the uncoated NMC shows the capacity of 102 $mAhg^{-1}$ for the first discharge. The capacity is continuously decreased with an increase in cycle number and degrades to be 74 $mAhg^{-1}$ after 250 cycles. Those results suggest that the $LiAlO_2$ coating improves the cell performance and the capacity retention for charge–discharge cycling.

Indeed, the $LiAlO_2$ coating is very effective to improve battery performance, but the energy density of the bulk-type solid-state cell is only about 15 $Whkg^{-1}$. The energy density of the cell was calculated from the total weights of the positive electrode composite, the solid electrolyte separator, and the negative electrode materials, excepting the weights of current collectors and the cases. Hence further improvement of the bulk-type test cell is needed to develop practical batteries.

In order to improve the energy density of the test cell and to estimate the limit of the loading amounts of the positive electrode composite, the test cells with a large amount of the electrode composite are examined. The schematic diagram of the test cell is illustrated in Fig. 5a. The weight of the positive electrode composite of the cell is 65 mg, which is about 4.5 times larger than that of the cell as shown in Fig. 2. The total weight of the cell is about 150 mg, excepting the weights of the current

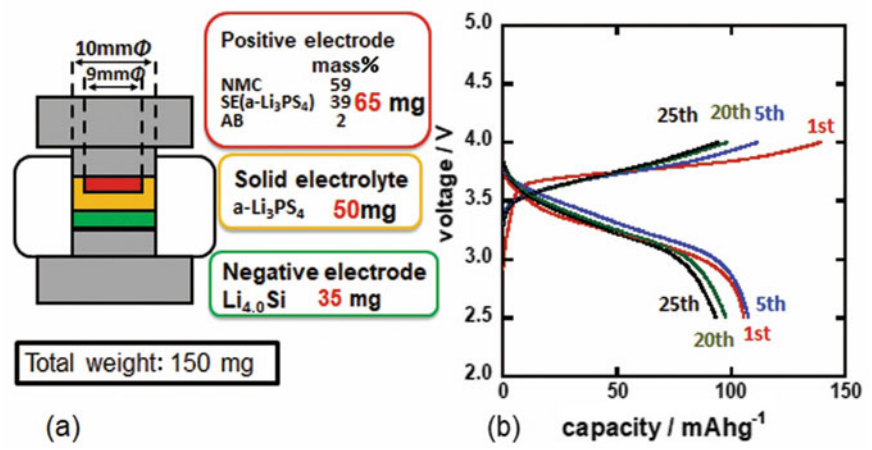

Fig. 5 **a** Schematic diagram of a solid-state test cell for high energy density. **b** Charge–discharge curves of the test cell at the current density of 0.1 $mAcm^{-2}$ at 25 °C

collectors and the cases. The charge–discharge cycle test was carried out under a constant current density of 0.1 $mAcm^{-2}$ at 25 °C. The charge–discharge curves of the cell with the large amount of the positive electrode composite are shown in Fig. 5b. The first discharge capacity of the test cell is about 110 $mAhg^{-1}$ and the energy density of the cell is 90 $Whkg^{-1}$ for the first discharge. The energy density is about six times larger than that of the cell shown in Fig. 2.

The charge–discharge cycle test was performed under several different current densities, 0.1, 0.4, 0.8 $mAcm^{-2}$. The current density was changed every five cycles. After the test with the current density of 0.8 $mAcm^{-2}$, the current density was changed back to the initial current density of 0.1 $mAcm^{-2}$. The cycle dependences of the charge and discharge capacities and typical discharge curves at those current densities are shown in Fig. 6a–b, respectively. The bulk-type solid-state cell with the large amount of the electrode composite, 65 mg, shows good performance even under the current density of 0.8 $mAcm^{-2}$. However, the capacity is decreased to 48 $mAhg^{-1}$ under the current density of 0.8 $mAcm^{-2}$. The deterioration of the capacity under the high current density would be related to the thick layer of the positive electrode. The thickness of the electrode layer is about 500 μm. The electrode layer would be too thick to operate the cell under the high current density. Those results suggest that there is a limit of the loading amount of the positive electrode composite in the bulk-type solid-state cells, and the limit of thickness of the positive electrode layer would be estimated to be 500 μm. Hence, layer-type solid-state cells, which have thin layer structure, are needed to develop solid-state batteries for practical uses.

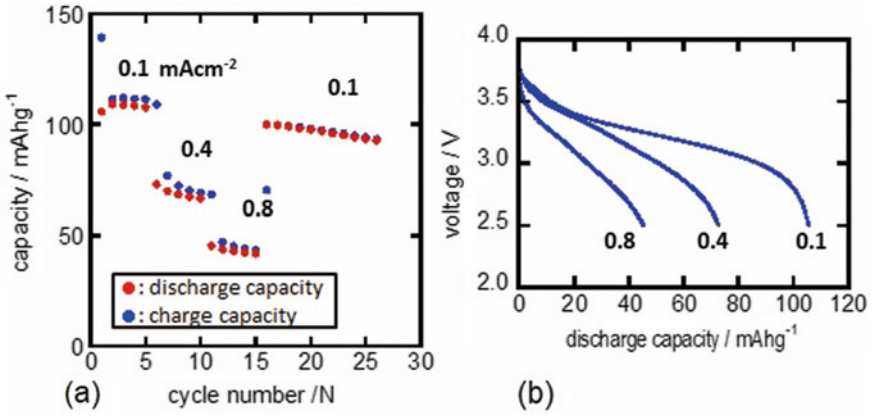

Fig. 6 **a** Cycle dependences of the charge and discharge capacities of the test cell with a large amount of positive electrode composite. **b** Typical discharge curves at the current densities of 0.1, 0.4, and 0.8 $mAcm^{-2}$

3 Solid Electrolyte-Coated Electrode Materials

The amount of solid electrolyte in the composite electrode is crucial to obtain a low interfacial electrode/electrolyte resistance, however, large amount of the solid electrolyte limits the total energy density of the batteries. In order to reduce the solid electrolyte content in the positive electrode composites and to achieve the good contact between solid electrolyte and positive electrode active materials, many researches were conducted on the solid electrolyte coating on the active materials by the use of dry [12, 13] and wet [14–18] processes. Here, a wet process is introduced as an example of solid electrolyte coating on active materials. Amorphous Li_3PS_4 solid electrolyte shows relatively high lithium-ion conductivity 4×10^{-4} Scm^{-1} at room temperature and a wide electrochemical window in the range of 0–5.0 V versus the Li^+/Li electrode. Hence, the amorphous Li_3PS_4 was selected as the coating solid electrolyte on the $LiNi_{1/3}Mn_{1/3}Co_{1/3}O_2$ (NMC) positive electrode materials.

The Li_3PS_4-coated NMC powder was prepared by the use of a three-step wet process. For the first step, the raw materials, Li_2S (Mitsuwa pure chemicals, 99.9%) and P_2S_5 (Sigma-Aldrich, 99%) were reacted in tetrahydrofuran (THF) for 24 h at room temperature. The mixture was concentrated under reduced pressure at 80 °C and the residual was obtained as a precursor of Li_3PS_4. The obtained precursor contains a little amount of THF. The remained THF causes the transformation of amorphous Li_3PS_4 into β-Li_3PS_4 crystalline phase, when the precursor is heated at high temperature to remove the remained THF. In order to solvent exchange THF for 1,2-diethoxyethane (DEE), in the second step, the precursor of Li_3PS_4 was added into DEE, which was used as a solvent and stirred for 48 h at room temperature. The slurry solution of $Li_3PS_4$with DEE was obtained. In the third step, the $LiNbO_3$-coated NMC powders were added into the slurry and ultrasonically agitated at 40 °C

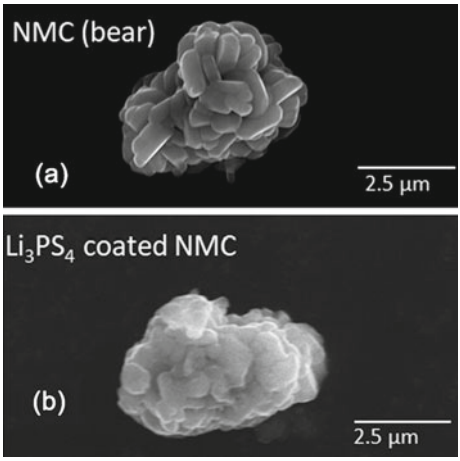

Fig. 7 FE-SEM images of **a** the uncoated $LiNi_{1/3}Mn_{1/3}Co_{1/3}O_2$ particle and **b** the 24.5 wt% Li_3PS_4-coated $LiNi_{1/3}Mn_{1/3}Co_{1/3}O_2$ particle

for 30 min. The $LiNbO_3$ coating is very effective to passivate the interdiffusion of transition metal and sulfur species at the boundary between NMC particle and Li_3PS_4 solid electrolyte. The interdiffusion of the transition metal and sulfur species causes the deterioration of the electrochemical performance of the active materials [9]. The slurry was prepared for the final products to have the Li_3PS_4 content in the range of 0–40 wt%. The mixture was concentrated under reduced pressure, and the residual was obtained as a precursor. The precursor was heated at 160 °C for 2 h and then the amorphous Li_3PS_4-coated NMC powders were obtained.

FE-SEM and energy dispersive X-ray (EDX) measurements were carried out in order to observe morphology of the uncoated NMC and the Li_3PS_4-coated NMC powders. Figure 7 displays FE-SEM images of the NMC particle coated with 24.5 wt% Li_3PS_4. Those NMC powders were heat-treated at 160 °C for 2 h in vacuo. The image of the uncoated NMC powder is also shown in the figure for comparison. For the uncoated NMC sample, as shown in Fig. 7a, the primary particle size is about 0.5–2.0 μm in diameter and those small particles aggregated each other to form spherical secondary particles about 5–8 μm in diameter. In the Li_3PS_4-coated sample, there are no significant differences in the surface morphology and in the particle size in the scale of the SEM observation. The Li_3PS_4-coated particle, however, has smooth surfaces and the surfaces can be attributed to Li_3PS_4.

The EDX mappings of the Li_3PS_4-coated NMC are depicted in Fig. 8. Both P and S atoms of Li_3PS_4 and Mn atom of NMC are detected in the same area. Those results indicate the formation of Li_3PS_4 layer on NMC particles. In addition, whitish particles that are denoted by dotted circles in Fig. 8a are newly observed and stick on the surface of the secondary particles of NMC. The newly appeared particles have smooth surfaces and can be attributed to Li_3PS_4.

Laboratory-scale solid-state cells were constructed with the obtained Li_3PS_4-coated NMC, amorphous Li_3PS_4 as the solid electrolytes, and $Li_{4.4}Si$ alloy as the negative electrode materials. The amorphous sulfide-based electrolyte, Li_3PS_4, was

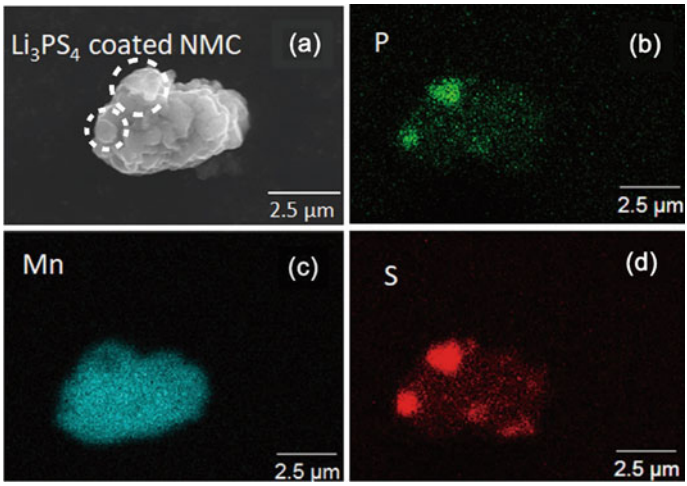

Fig. 8 **a** FE-SEM image of the 24.5 wt% Li_3PS_4-coated NMC particle. The EDX mappings of the 24.5 wt% Li_3PS_4-coated NMC particle for **b** P, **c** Mn, and **d** S atoms obtained from the same field of the SEM image

synthesized by the wet process without the third step already described above. The Li_3PS_4 was used as the electrochemical separator between the positive and negative electrodes. The synthesized Li_3PS_4 shows high lithium-ion conductivity, 2×10^{-4} Scm^{-1} at room temperature. The positive electrode of the test cell was a mixture of the obtained Li_3PS_4-coated NMC (98 wt%) and acetylene black (2 wt%). The test cell was prepared by successively pressing the positive electrode mixture, the Li_3PS_4 solid electrolyte powder, and the $Li_{4.4}Si$ alloy powder at 380 MPa into a pellet of 10 mm diameter. In order to elucidate the effect of the Li_3PS_4 coating on the active materials, the test cell with the composite of the non-coated NMC, Li_3PS_4 which was separately synthesized as solid electrolytes, and acetylene black (2 wt%) was also constructed. In this case, the composite electrode has the same Li_3PS_4 content as the electrode with the Li_3PS_4-coated NMC.

Galvanostatic charge–discharge cycling tests of the cells were performed under a constant current density of 0.1 $mAcm^{-2}$ at 298 K. Figure 9 shows the first charge–discharge curves of the bulk-type test cell with the Li_3PS_4-coated NMC. The positive electrode composite contains 24.5 wt% Li_3PS_4. The first charge–discharge curves of the test cell with the non-coated NMC are also shown in the figure for comparison. The positive electrode with non-coated NMC contains the same amounts of Li_3PS_4 as that with the Li_3PS_4-coated NMC. In the charge process, both test cells with the Li_3PS_4-coated and with the non-coated NMCs show almost same properties. The charge capacities of both test cells are about 160 $mAhg^{-1}$. On the other hand, in the discharge process, the test cell with the Li_3PS_4-coated NMC shows a higher discharge capacity of 140 $mAhg^{-1}$ than the test cell with the non-coated NMC, which shows the discharge capacity of about 120 $mAhg^{-1}$. The discharge process induces the volume shrinkage of NMC particles and the shrinkage separates some portions of the active

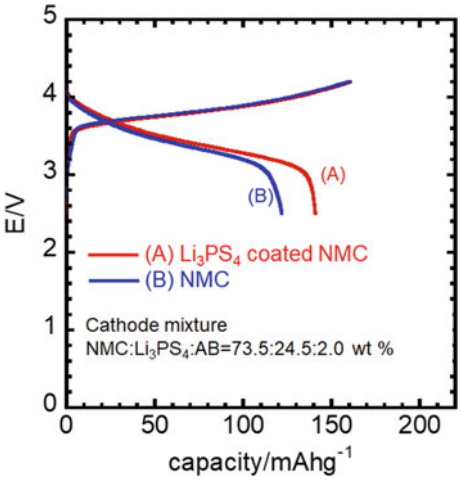

Fig. 9 The first charge–discharge curves of the test cells (**A**) with the 24.5 wt% Li_3PS_4-coated NMC and (**B**) with the uncoated NMC

materials NMC from the solid electrolyte Li_3PS_4 in the composite electrode. The breaking contact between the active materials and solid electrolyte in the electrode composite should cause the decrease in the discharge capacity. Those results indicate that the Li_3PS_4-coated NMC would have the excellent close contactness between the Li_3PS_4 solid electrolyte and the NMC active materials in the positive electrode composite.

Figure 10a shows the Li_3PS_4-content dependence of the discharge capacity of the Li_3PS_4-coated NMC. The discharge capacity is calculated on the base of the weight of NMC contained in the positive electrode composites. The discharge capacity of the

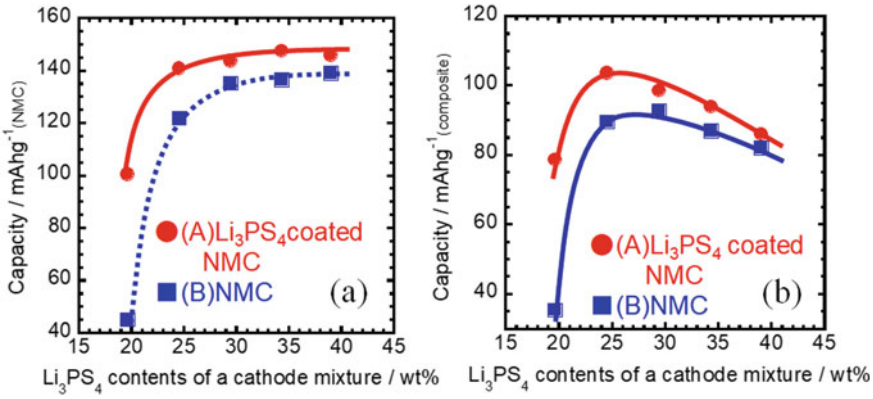

Fig. 10 Li_3PS_4 content dependences of the first discharge capacities of the bulk-type solid-state cells with the uncoated NMC and with the Li_3PS_4-coated NMC; **a** the discharge capacities were calculated on the base of weight of the NMC contained in the positive electrodes and **b** the discharge capacities were calculated on the base of the total weights of the positive electrodes

non-coated NMC is also shown in the figure for comparison. The capacity is increased with an increase in the Li_3PS_4 contents and reaches almost a constant capacity of about 145 $mAhg^{-1}$ for the cell with the Li_3PS_4-coated NMC. The capacities of the Li_3PS_4-coated NMC are larger than those of the non-coated NMC all over the composition range of 19–40 wt%.

The discharge capacity that is calculated on the base of the total weight of the composite electrode is shown in Fig. 10b as a function of the Li_3PS_4 contents. In this case, the discharge capacity shows the maximum of 105 $mAhg^{-1}$ at around the Li_3PS_4 content 25 wt%. The capacity of the non-coated NMC is also shown the maximum at the same composition range. However, the maximum capacity of the non-coated NMC is about 90 $mAhg^{-1}$ and is smaller than that of the Li_3PS_4-coated NMC. Those results suggest that the all-solid-state battery with the Li_3PS_4-coated NMC should have larger specific energy density than that with the non-coated NMC with the same Li_3PS_4 content. Hence, the solid-electrolyte coating on the active materials such as NMC is an effective way to develop all-solid-state lithium-ion batteries that have high energy density.

References

1. Minami, T. (2005). *Solid state ionics for batteries.* Tokyo: Springer.
2. Kamaya, N., Homma, K., Yamakawa, Y., Hirayama, M., Kanno, R., Yonemura, M., et al. (2011). *Nature Materials, 10,* 682–686.
3. Richards, W. D., Miara, L. J., Wang, Y., Kim, J. C., & Ceder, G. (2016). *Chemistry of Materials, 28,* 266–273.
4. Takada, K. (2013). *Acta Materialia, 61,* 759–770.
5. Ohta, N., Takada, K., Zhang, L. Q., Ma, R. Z., Osada, M., & Sasaki, T. (2006). *Advanced Materials, 18,* 2226–2229.
6. Takada, K., Ohta, N., Zhang, L., Fukuda, K., Sakaguchi, I., Ma, R., et al. (2008). *Solid State Ionics, 179,* 1333–1337.
7. Takada, K., Ohta, N., Zhang, L., Xu, X., Hang, B. T., Ohnishi, T., et al. (2012). *Solid State Ionics, 225,* 594–597.
8. Sakuda, A., Kitaura, H., Hayashi, A., Tadanaga, K., & Tatsumisago, M. (2009). *Journal of the Electrochemical Society, 156,* A27–A32.
9. Sakuda, A., Hayashi, A., & Tatsumisago, M. (2010). *Chemistry of Materials, 22,* 949–956.
10. Machida, N., Kashiwagi, J., Naito, N., & Shigematsu, T. (2012). *Solid State Ionics, 225,* 354–358.
11. Okada, K., Machida, N., Naito, N., Shigematsu, T., Ito, S., Fujiki, S., et al. (2014). *Solid State Ionics, 255,* 120–127.
12. Sakuda, A., Hayashi, A., Ohtomo, T., Hama, S., & Tatsumisago, M. (2011). *Journal of Power Sources, 196,* 6735–6741.
13. Ito, Y., Otoyama, M., Hayashi, A., Ohtomo, T., & Tatsumisago, M. (2017). *Journal of Power Sources, 360,* 328–335.
14. Yubuchi, S., Teragawa, S., Aso, K., Tadanaga, K., Hayashi, A., & Tatsumisago, M. (2015). *Journal of Power Sources, 293,* 941–945.
15. Rosero-Navarro, N. C., Kinoshita, T., Miura, A., Higuchi, M., & Tadanaga, K. (2017). *Ionics, 23,* 1619–1624.
16. Phuc, N. H. H., Morikawa, K., Mitsuhiro, T., Muto, H., & Matsuda, A. (2017). *Ionics, 23,* 1–7.

17. Rosero-Navarro, N. C., Miura, A., & Tadanaga, K. (2018). *Journal of Power Sources, 396,* 33–40.
18. Yubuchi, S., Uematsu, M., Hotehama, C., Sakuda, A., Hayashi, A., & Tatsumisago, M. (2019). *Journal of Materials Chemistry A, 7,* 558–566.